

Article

Not peer-reviewed version

Highly Sensitive Titanium-Based MXene-Reduced Graphene Oxide Composite for Efficient Electrochemical Heavy Metal Detection of Cadmium and Copper Ions in Water

Dharshini Mohanadas , [Rosiah Rohani](#) ^{*} , Siti Fatimah A Rahman , Ebrahim Mahmoudi , Yusran Sulaiman

Posted Date: 31 March 2025

doi: 10.20944/preprints202503.2229.v1

Keywords: Titanium-based MXene; graphene; electrochemical analysis; electrochemical sensor; heavy metals detection



Preprints.org is a free multidisciplinary platform providing preprint service that is dedicated to making early versions of research outputs permanently available and citable. Preprints posted at Preprints.org appear in Web of Science, Crossref, Google Scholar, Scilit, Europe PMC.

Copyright: This open access article is published under a Creative Commons CC BY 4.0 license, which permit the free download, distribution, and reuse, provided that the author and preprint are cited in any reuse.

Article

Highly Sensitive Titanium-Based MXene-Reduced Graphene Oxide Composite for Efficient Electrochemical Detection of Cadmium and Copper Ions in Water

Dharshini Mohanadas^{1,3}, Rosiah Rohani^{1,2,*}, Siti Fatimah A Rahman¹, Ebrahim Mahmoudi^{1,2} and Yusran Sulaiman^{3,4}

¹ Department of Chemical & Process Engineering, Faculty of Engineering and Built Environment, Universiti Kebangsaan Malaysia, UKM, Bangi 43600, Selangor, Malaysia

² Research Centre for Sustainable Process Technology, Faculty of Engineering & Built Environment, Universiti Kebangsaan Malaysia, UKM, Bangi 43600, Selangor, Malaysia

³ Department of Chemistry, Faculty of Science, Universiti Putra Malaysia, UPM Serdang, 43400, Selangor, Malaysia

⁴ Functional Nanotechnology Devices Laboratory, Institute of Nanoscience and Nanotechnology (ION2), Universiti Putra Malaysia, UPM, 43400 Serdang, Selangor, Malaysia

* Correspondence: author E-mail address*: rosiah@ukm.edu.my

Abstract: A simple and efficient synthesis route was introduced to develop an electrochemically active and promising binary composite that was made up of titanium based MXene ($\text{Ti}_3\text{C}_2\text{T}_x$) and rGO to simultaneously detect ions namely Cd^{2+} and Cu^{2+} in water. XRD, FTIR, Raman, XPS, FESEM, elemental mapping and EDX analysis affirmed successful formation of $\text{Ti}_3\text{C}_2\text{T}_x$ -rGO composite. The produced $\text{Ti}_3\text{C}_2\text{T}_x$ -rGO electrode exhibited an homogeneous rGO sheet covered $\text{Ti}_3\text{C}_2\text{T}_x$ MXene plates with the all the detailed $\text{Ti}2p$, $\text{C}1s$ and $\text{O}1s$ XPS peaks. The high performance $\text{Ti}_3\text{C}_2\text{T}_x$ -rGO composite was successfully tested Cd^{2+} and Cu^{2+} ions via differential pulse voltammetry (DPV), altering the pH, concentration and the real water sample quality. The electrochemical performances revealed that the proposed $\text{Ti}_3\text{C}_2\text{T}_x$ -rGO composite depicted very low detection and quantification limits (LOD and LOQ) respectively, both for Cd^{2+} (LOD = 0.31 nM, LOQ = 1.02 nM) and Cu^{2+} (LOD = 0.18 nM, LOQ = 0.62 nM) ions, where the result is highly comparable with the reported literature. The $\text{Ti}_3\text{C}_2\text{T}_x$ -rGO is proven highly sensitive towards Cd^{2+} ($0.345 \mu\text{M}\mu\text{A}^{-1}$) and Cu^{2+} ($0.575 \mu\text{M}\mu\text{A}^{-1}$) with great repeatability and reproducibility properties. $\text{Ti}_3\text{C}_2\text{T}_x$ -rGO electrode was also exhibited excellent stability over four weeks with the retention of 97.86% and 98.01% for Cd^{2+} and Cu^{2+} , respectively. This simple approach on modifying $\text{Ti}_3\text{C}_2\text{T}_x$ utilizing rGO can potentially be advantageous in the development of highly sensitive electrochemical sensors for simultaneous detection of heavy metal ions.

Keywords: Titanium-based MXene; graphene; electrochemical analysis; electrochemical sensor; heavy metals detection

1. Introduction

"Environmental health hazards" are identified based on the toxicity of the substance and potential exposure to contaminated air, water, soil, and heavy metal ions. It is also classified in the top ten list of the "Agency for Toxic Substances and Disease Registry Priority List of Hazardous Substances" [1]. The most abundant forms of water pollutants that result in negative effects on ecosystems, marine animals, and human health are heavy metals, such as copper (Cu), lead (Pb), cadmium (Cd), chromium (Cr), mercury (Hg), and zinc (Zn). Many detection methods have been invented due to the increasing demand for a better evaluation of the quality of water, specifically in

respect to heavy metal contamination. The three distinct types of these heavy metal detection approaches are spectroscopic, electrochemical, and optical detection. In comparison, the electrochemical approach is emphasized for identifying heavy metal as it requires quick analytical time and cheap and easy equipment/operation great sensitivity and possesses excellent selectivity [2, 3].

MXene consists of metal carbide, nitride, or carbonitride nanosheet in a two-dimensional (2D) transition material. Meanwhile $\text{Ti}_3\text{C}_2\text{T}_x$ is a titanium based MXene, an extensively developed and explored MXene to be employed in the treatment of water [4]. $\text{Ti}_3\text{C}_2\text{T}_x$ MXene has been developed by researchers for identifying heavy metals, specifically for the detection of Cu^{2+} , Cr^{7+} , Ba^{2+} , and Pb^{2+} utilizing in-situ reductions and adsorption technique. MXene has strong catalytic activity against a variety of water contaminants in the sensing application, in the presence of -O and -OH functional groups, which provide an abundance of active sites for a direct ion-exchange process. Shahzad *et al.* [5] proposed a 2D $\text{Ti}_3\text{C}_2\text{T}_x$ nanosheet that has active interaction with Cu^{2+} ions, to produce adsorption capacity of 2.7 times bigger than the typically accessible activated carbon. The introduction of $\text{Ti}_3\text{C}_2\text{T}_x$ MXene nanoribbons drastically enhance the adsorption and reduction properties, where promising and simple electrochemical analysis demonstrate an excellent LOD of 0.94 nM for Cd^{2+} ion [6]. The alkalized $\text{Ti}_3\text{C}_2\text{T}_x$ ($\text{Ti}_3\text{C}_2(\text{OH}/\text{ONa})_x\text{F}_{2-x}$) electrode comprises multiple active Ti-O and Ti-OH sites also demonstrated promising signal towards the Pb^{2+} purification for environmental remediation [7]. On the other hand, the diverse $\text{Ti}_3\text{C}_2\text{T}_x$ MXene layer possesses a restricted distance within the multiple sheets inhibits electrode performance. This is due to only a tiny portion of the electroactive sites are attached in the detecting process. Modification of the surface is a viable strategy for improving MXene characteristics for offering potential sensing performance as this can drastically increase MXene layer distance. MXene has been altered using numerous electroactive components such as conductive polymers, transition metal oxide, graphene in order to boost the sensing properties. Xia *et al.*, [8] incorporated carbon black with $\text{Ti}_3\text{C}_2\text{T}_x$ MXene and the result revealed that the aggregation of $\text{Ti}_3\text{C}_2\text{T}_x$ MXene has been successfully prevented and the electron transfer as well as the electrode surface area has been gradually improved via the proposed modification. It is also proven that the simultaneous detection heavy metal ions is promisingly high for nitrogen and phosphorus co-doped $\text{Ti}_3\text{C}_2\text{T}_x$ MXene electrode as the dopants significantly boost the accessible electroactive region of the electrode in simultaneously detecting Cu^{2+} and Hg^{2+} [9].

Among numerous candidates, the electrochemically conductive and mechanically stable reduced graphene oxide (rGO) is an ideal candidate for heavy metal sensing in water. A thermally produced rGO thin film was presented by Maity *et al.* [10] for rapid Pb^{2+} ion detection in various water sources. An excellent Pb^{2+} detection in a 1 M HCl solution and common water samples were revealed employing an electrochemically developed rGO of graphite enforced carbon material. [11]. The lowest LOD ($\text{Pb}^{2+} = 0.1 \text{ g/L}$ and $\text{Cd}^{2+} = 1.0 \text{ g/L}$) were observed for simultaneous heavy metal ions, utilizing the micro-patterned rGO, which was effectively fabricated utilizing lithography approach [12]. Researchers discovered that the restored sp^2 carbon network in the rGO structure leads to enhanced electro-conductivity [13]. The rGO structure bound with amino groups has improved the electrode of the electrically active area. Hence, rGO can be incorporated with the $\text{Ti}_3\text{C}_2\text{T}_x$ to significantly boost the electrochemical performance of the electroactive material for identifying the presence of heavy metals in water. This is because the surface area of $\text{Ti}_3\text{C}_2\text{T}_x$ MXene is significantly accessible during the process of detection, where rGO potentially serves as the spacer as well as anti-pile layer, eventually offering greater electroactive sites.

In the present work, a promising binary composite that consists of titanium based MXene ($\text{Ti}_3\text{C}_2\text{T}_x$) and rGO was homogeneously prepared via sonication approach for instantaneous identification of Cu^{2+} and Cd^{2+} in water. The properties of the as-prepared $\text{Ti}_3\text{C}_2\text{T}_x$ -rGO composite morphological structure was characterized using XRD, FTIR, Raman, FESEM, EDX and XPS. The developed $\text{Ti}_3\text{C}_2\text{T}_x$ -rGO was optimized by varying the ratio of $\text{Ti}_3\text{C}_2\text{T}_x$ and rGO. The optimized electroactive material was utilized for a simultaneous detection of Cd^{2+} and Cu^{2+} ions in water. $\text{Ti}_3\text{C}_2\text{T}_x$ -rGO is expected to exhibit a promising limit of detection of heavy metals and an excellent

limit of quantification of them, with great electrode sensitivity. $\text{Ti}_3\text{C}_2\text{T}_x\text{-rGO}$ is also illustrates a still high peak current retention after a long period of usage, signifying an outstanding electrode stability.

2. Materials and Methods

2.1. Materials

Potassium chloride (KCl, 99%) as well as sulphuric acid (H_2SO_4 , 96%) were acquired from Fisher scientific. Meanwhile, dikalium hydrogen phosphate (K_2HPO_4 , 98%), kalium dihydrogen phosphate (KH_2PO_4 , 98%) and nitric acid (HNO_3 , 65%) were obtained from Merck KGaA. Sigma Aldrich supplied graphene oxide (GO, 4 mg/mL) and polyvinylidene fluoride (PVDF), Titanium aluminum carbide (Ti_3AlC_2 , 90%), lithium fluoride (LiF, 97%), hydrochloric acid (HCl, 37%), ethanol (95%), cadmium (II) chloride (CdCl_2 , 99.9%), and copper (II) chloride (CuCl_2 , 99.9%). Milli-Q deionized (DI) water was obtained from Millipore (18.5 M Ω .cm, 25°C).

2.2. Preparation of $\text{Ti}_3\text{C}_2\text{T}_x\text{-rGO}$ Nanocomposite

The layered $\text{Ti}_3\text{C}_2\text{T}_x$ MXene was produced from the etching approach of the aluminium phase of MAX Ti_3AlC_2 . Firstly, the etching solution was obtained by mixing LiF (1.0 g) in 9 mol/L HCl (20 mL) solution, utilizing magnetic stirring (30 min) approach. Then, 1.0 g of Ti_3AlC_2 was slowly added into the prepared mixture and allowed to stir continuously (24 h) at 35°C to attain an impure $\text{Ti}_3\text{C}_2\text{T}_x$ MXene solvent. The collected impure $\text{Ti}_3\text{C}_2\text{T}_x$ MXene was washed with the DI water and followed by centrifuge (3500 rpm) for 10 min until it reached pH > 6.0. The pure $\text{Ti}_3\text{C}_2\text{T}_x$ MXene nanosheet dispersion was then allowed to dry utilizing a freeze dryer.

The $\text{Ti}_3\text{C}_2\text{T}_x\text{-rGO}$ nanocomposite was fabricated via sonication and followed by electrochemical reduction (Figure 1(a)). First, the $\text{Ti}_3\text{C}_2\text{T}_x$ dispersion (3 mg/mL) was prepared by magnetically stirring $\text{Ti}_3\text{C}_2\text{T}_x$ powder (15 mg) with DI water (5 mL) for 30 min. The 3 mg/mL GO solution that sonicated for 1 h was then mixed with the 5 mL $\text{Ti}_3\text{C}_2\text{T}_x$ dispersion and proceed with ultrasonic treatment for 1 h. The prepared dispersion (5 μL) was drop casted on a clean glassy carbon electrode (GCE) surface and allowed to dry at room temperature. GCE was polished on the polishing cloth, employing 0.5 μm of alumina slurry. The GCE was later sonicated for 10 minutes with HNO_3 and deionized water to obtain a clean electrode surface. The dried $\text{Ti}_3\text{C}_2\text{T}_x\text{-GO}$ modified GCE was electrochemically treated in the PBS solution (pH 7), and performed a chronoamperometry method (-0.8 V) for 3 min [14, 15]. The produced $\text{Ti}_3\text{C}_2\text{T}_x\text{-rGO}$ nanocomposite was labelled as the working electrode in this application. The digital pictures in Figure 1(b) clearly differentiates the surface of GCE via electrode modification.

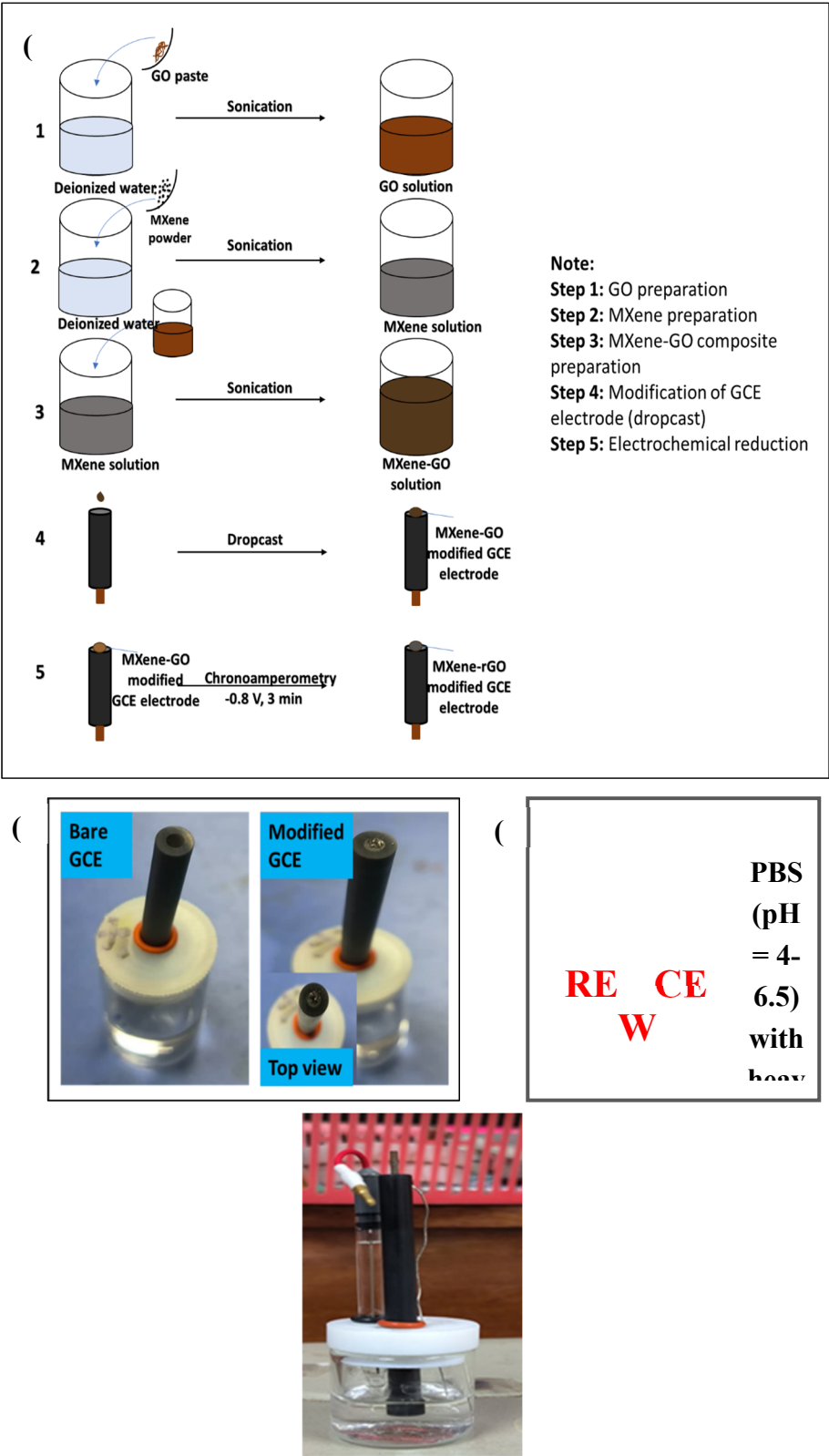


Figure 1. (a) Schematic diagram illustrates the synthesis of $Ti_3C_2T_x$ -rGO nanocomposite. (b) Digital photographs demonstrate the surface of GCE before (left) and after (right) modification process. (c) The three-electrode system setup of the electrodes for electrochemical analysis (pH study).

2.3. $Ti_3C_2T_x$ -rGO Nanocomposite Characterization

X-ray diffraction analysis was conducted to examine the phase composition of the synthesized samples using Bruker X-ray diffractometer D8 advance. The vibration modes and functional groups signals of the materials were retrieved from Raman spectroscopy (Thermo Scientific Raman

spectrometer, 488 nm) and Fourier Transform Infrared Spectrometer (FTIR, Perkin-Elmer Spectrum100), respectively. The field emission scanning microscopy (FESEM, ZEISS MERLIN) and X-ray photoelectron spectroscopy (XPS, XSAMHS Kratos Analytical) were performed to determine the morphology and the chemical composition of the composite surfaces, respectively.

2.4. Electrochemical Detection of Heavy Metals

The prepared binary $\text{Ti}_3\text{C}_2\text{T}_x$ -rGO was investigated for simultaneous heavy metal detection namely, Cd^{2+} , and Cu^{2+} ions. Various analysis was conducted to investigate the performance of $\text{Ti}_3\text{C}_2\text{T}_x$ -rGO on the detection of analytes. All electrochemical analyses were performed via potentiostat (Autolab PGSTAT204) utilizing electroactive material coated GCE (working electrode), platinum (Pt) wire (counter electrode) and silver/silver chloride (Ag/AgCl, reference electrode); in a three-electrode configuration). Differential pulse voltammetry (DPV) assessments were conducted for the proposed $\text{Ti}_3\text{C}_2\text{T}_x$ -rGO electrode at the potential ranging from -0.95 to -0.05 V for all the analysis (pH study, concentration study, real sample study, interference study, reproducibility test, repeatability test, stability test) in the sensor application. In this work, the detection of copper (Cu^{2+}) and cadmium (Cd^{2+}) ions using a MXene/rGO composite electrode via Differential Pulse Voltammetry (DPV) is typically carried out under careful optimized experimental conditions to achieve high sensitivity and selectivity towards the heavy metal detection. The actual experimental conditions of this work were properly developed following strict and standard procedures that are commonly conducted. The effect of supporting electrolyte pH on the voltammetric response of the mixture of Cd^{2+} , and Cu^{2+} on the prepared electrode was evaluated in the phosphate buffer solution (PBS) in pH 4-6.5 (Figure 1(c)). DPV was performed to record the pH effect for the detection.

The concentration study was carried out by increasing the concentration of both analyte (Cd^{2+} , and Cu^{2+}) in the optimized condition. A calibration curve was obtained from the relation between same analyte concentration against the produced oxidation peak current and the error bars (relative standard deviation) were generated for each concentration of analyte. This analysis was conducted via DPV method at 50 mV pulse amplitude, 50 ms pulse width and 20 mV/s scan rate. The reproducibility of electrochemical sensor was examined by measuring the analytes using five different electrodes and the relative standard deviation (RSD) was calculated. Repeatability of the sensor was evaluated by recording ten successive measurements using same electrode. Stability of the electrochemical sensor was studied by preparing different electrodes and store it at the room temperature for a period. The current response of the stored electrodes was recorded after 1 week, 2 weeks, 3 weeks and 4 weeks via DPV analysis. The percentage of signal change was calculated and compared for all 4 weeks.

3. Result and Discussion

3.1. Characterization

Figure 2 demonstrates XRD diffraction peaks of various samples. This analysis was conducted to determine the sample phase compositions. The Ti_3AlC_2 illustrates XRD diffraction peaks at 9.5° (002), 18.9° (004), 34.0° (101), 38.9° (104), 41.8° (105), 48.4° (107), 56.5° (109) and 60.7° (110), which matches well with the JCPDS pattern 052-0875 of Ti_3AlC_2 (hexagonal lattice) [16]. The $\text{Ti}_3\text{C}_2\text{T}_x$ MXene produced through etching process demonstrates (002), (004), (101), (104), (105), (107), (109) and (110) planes at 8.3° , 19.1° , 34.0° , 38.7° , 41.8° , 48.4° , 56.4° and 60.5° . The diminished (104) plane of $\text{Ti}_3\text{C}_2\text{T}_x$ and the (002) plane of $\text{Ti}_3\text{C}_2\text{T}_x$ MXene is noticeably lower in intensity and broader peak at 8.3° , signifying the successful Al-etching of Ti_3AlC_2 [17, 18]. GO illustrates a diffraction peak at 10.2° , indicating the lattice plane (001) [19-21]. The effective electrochemical reduction procedure results in a wide rGO diffraction peak of $2\theta = 25.3^\circ$ (002), implying the presence of graphite-like sheets [14, 22, 23]. The $\text{Ti}_3\text{C}_2\text{T}_x$ -rGO illustrates all XRD signals of $\text{Ti}_3\text{C}_2\text{T}_x$ and rGO, validating a successful formation of the sample.

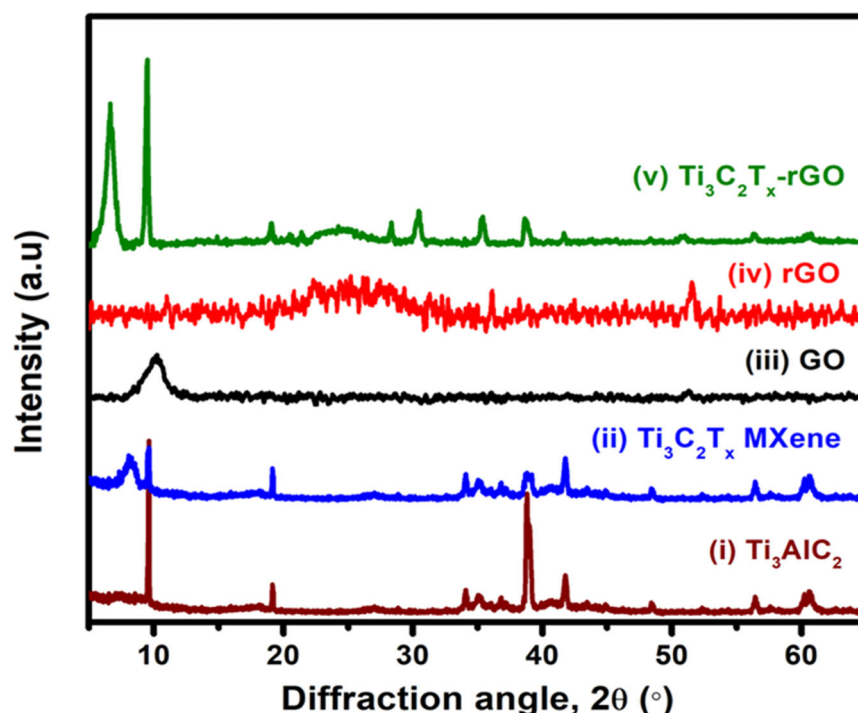


Figure 2. XRD spectra of Ti_3AlC_2 , $\text{Ti}_3\text{C}_2\text{T}_x$ MXene, GO, rGO and $\text{Ti}_3\text{C}_2\text{T}_x\text{-rGO}$.

The vibration modes within the as-prepared materials were investigated via Raman spectroscopy (Figure 3(a)). Strong D band (sp^3 -hybridized carbon) and G band (sp^2 -hybridized carbon) are observed for GO (D band= 1355 cm^{-1} and G band= 1594 cm^{-1}) and rGO (D band= 1354 cm^{-1} and G band= 1594 cm^{-1}) samples. The band intensity ratio of D over G (I_D/I_G) can be adopted to estimate the degree of disorder in the graphite structure. The ratio value of I_D/I_G larger than 1 signifies that the sample comprises more sp^3 -hybridized carbon atoms than sp^2 -hybridized carbons [24-26]. The measured I_D/I_G ratio of GO is 0.94, whereas the I_D/I_G ratio of rGO (1.24) and $\text{Ti}_3\text{C}_2\text{T}_x\text{-rGO}$ (1.32) confirm that the proposed electrochemical reduction process diminished oxygenated functional groups initially presence at the GO layer [27]. $\text{Ti}_3\text{C}_2\text{T}_x$ MXene depicts Raman peaks at 147.8, 279.4, 391.5, 591.0 cm^{-1} correspond to the low levels of anatase TiO_2 on the outermost surface of $\text{Ti}_3\text{C}_2\text{T}_x$ MXene [28]. The Raman signal at 721.8 shows the A_{1g} symmetrical out-of-plane vibration of Ti and C atoms [29]. The D band and G band of $\text{Ti}_3\text{C}_2\text{T}_x$ MXene are observed at 1325.2 and 1559.8 cm^{-1} , where the D band represents disorder induction within the structure. The synthesized $\text{Ti}_3\text{C}_2\text{T}_x\text{-rGO}$ illustrates all the characteristic peaks of $\text{Ti}_3\text{C}_2\text{T}_x$ and rGO.

Figure 3(b) represents the FTIR spectra of GO, rGO, $\text{Ti}_3\text{C}_2\text{T}_x$ MXene, and $\text{Ti}_3\text{C}_2\text{T}_x\text{-rGO}$ electrodes. GO demonstrates C-O-C, C=C, C=O and O-H functional groups at 1057, 1387, 1621 and 3301 cm^{-1} . After reduction reaction, rGO illustrates peaks at 1047 cm^{-1} (C-OH), 1363 cm^{-1} (C=C), 1597 cm^{-1} (C=O) and 3307 cm^{-1} (O-H). The intensity of O-H (3307 cm^{-1}) stretching mode of the carboxyl group of rGO is noticeably smaller than the GO (3301 cm^{-1}), validating successful electrochemical reduction process. The deformation vibration of Ti-O bond and C=O of $\text{Ti}_3\text{C}_2\text{T}_x$ MXene is detected at the respective peaks of 667 and 1640 cm^{-1} . The existence of hydroxyl groups is verified by the absorption signals at 3301 and 1640 cm^{-1} , which are ascribed to the absorbed external water and highly hydrogen-bonded OH or exceptionally strong coordinated H_2O in the $\text{Ti}_3\text{C}_2\text{T}_x$ MXene. The detected FTIR signal of $\text{Ti}_3\text{C}_2\text{T}_x\text{-rGO}$ further affirms the formation of the composite.

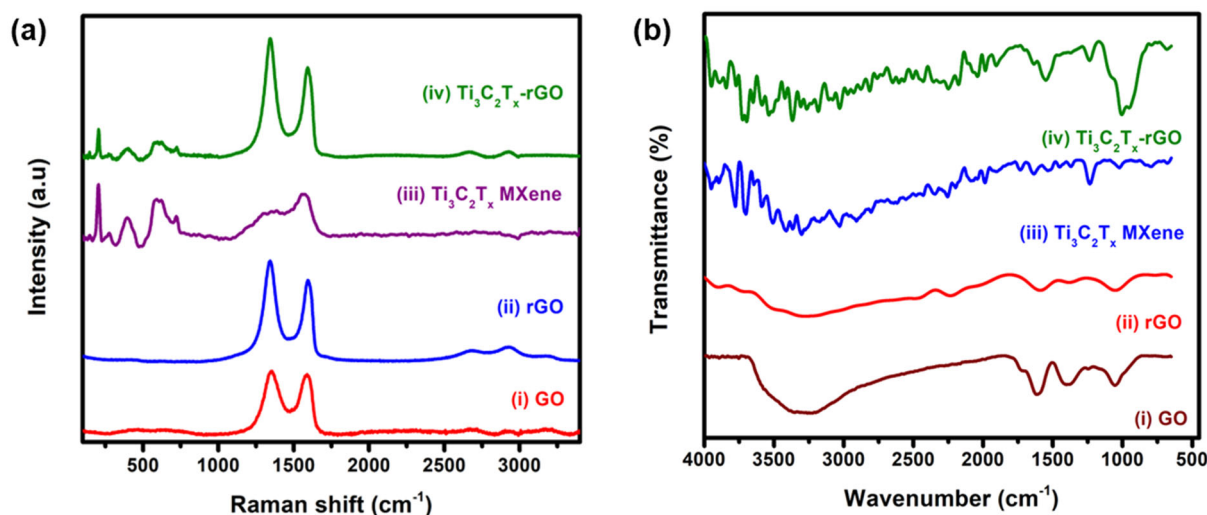


Figure 3. (a) Raman and (b) FTIR spectra of GO, rGO, Ti₃C₂T_x MXene, and Ti₃C₂T_x-rGO.

Identification of the surface morphology of the as-prepared samples was performed using FESEM analysis and presented in Figure 4. Both GO (Figure 4a(i)) and rGO (Figure 4a(ii)) illustrate wrinkle-like morphology. The inset of Figure 4a(i-ii) denotes that the rGO has a more pronounced wrinkle-like morphology compared to the GO, which is the result of the electrochemical reduction process [19, 30, 31]. This statement is in good agreement with the XRD, FTIR and Raman results. Ti₃C₂T_x (Figure 4a(iii)) depicts a multi layered MXene flakes morphology after a successful chemical etching. Whereas, the Ti₃C₂T_x-rGO composite which prepared through simple sonication method shows that the rGO sheet uniformly covers the multi layered MXene flakes.

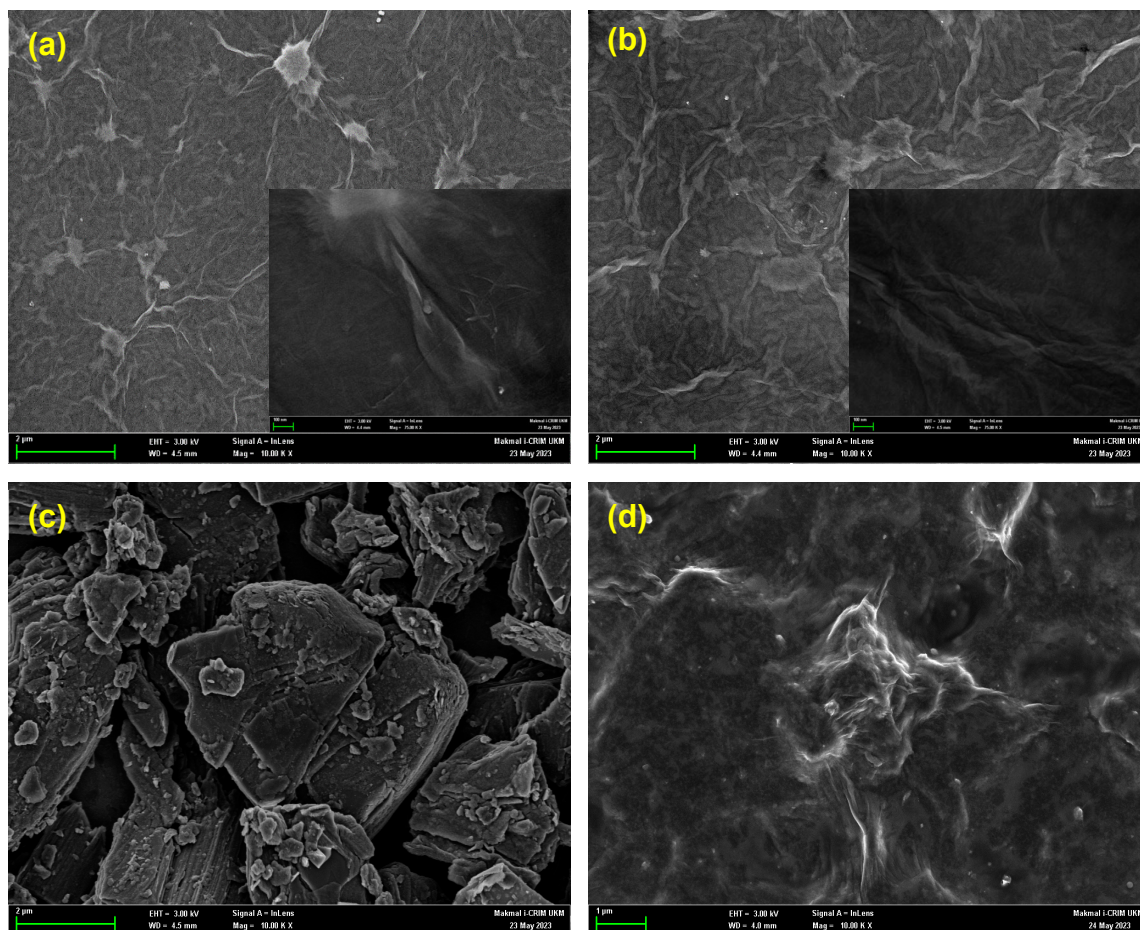


Figure 4. FESEM images of (a) GO (inset: GO at higher magnification), (b) rGO (inset: rGO at higher magnification), (c) $\text{Ti}_3\text{C}_2\text{T}_x$, and (d) $\text{Ti}_3\text{C}_2\text{T}_x$ -rGO.

$\text{Ti}_3\text{C}_2\text{T}_x$ -rGO composite was further evaluated through elemental mapping as depicted in Figure 5(a). Titanium (Ti), Carbon (C), Oxygen (O) and Aluminum (Al) are noticed from the analysis, and it can be clearly spotted that the all the elements are distributed evenly on the composite, confirming homogeneous formation of the composite. The Al signal still can be observed in the $\text{Ti}_3\text{C}_2\text{T}_x$ -rGO composite even after the Al-etching, which indicate that there is incomplete etching process at the inner layers of Ti_3AlC_2 [32]. From the EDX analysis (Figure 5(b)) of $\text{Ti}_3\text{C}_2\text{T}_x$ -rGO composite, Ti, C, O, and Al are successfully recorded with the respective weight percentage of 88.1, 10.3, 1.5 and 0.1%. EDX result revealed that only minimal amount of Al (0.1%) present within the composite, confirming a successful etching of Al and there is still few unetched Al within the inner structure of $\text{Ti}_3\text{C}_2\text{T}_x$ MXene.

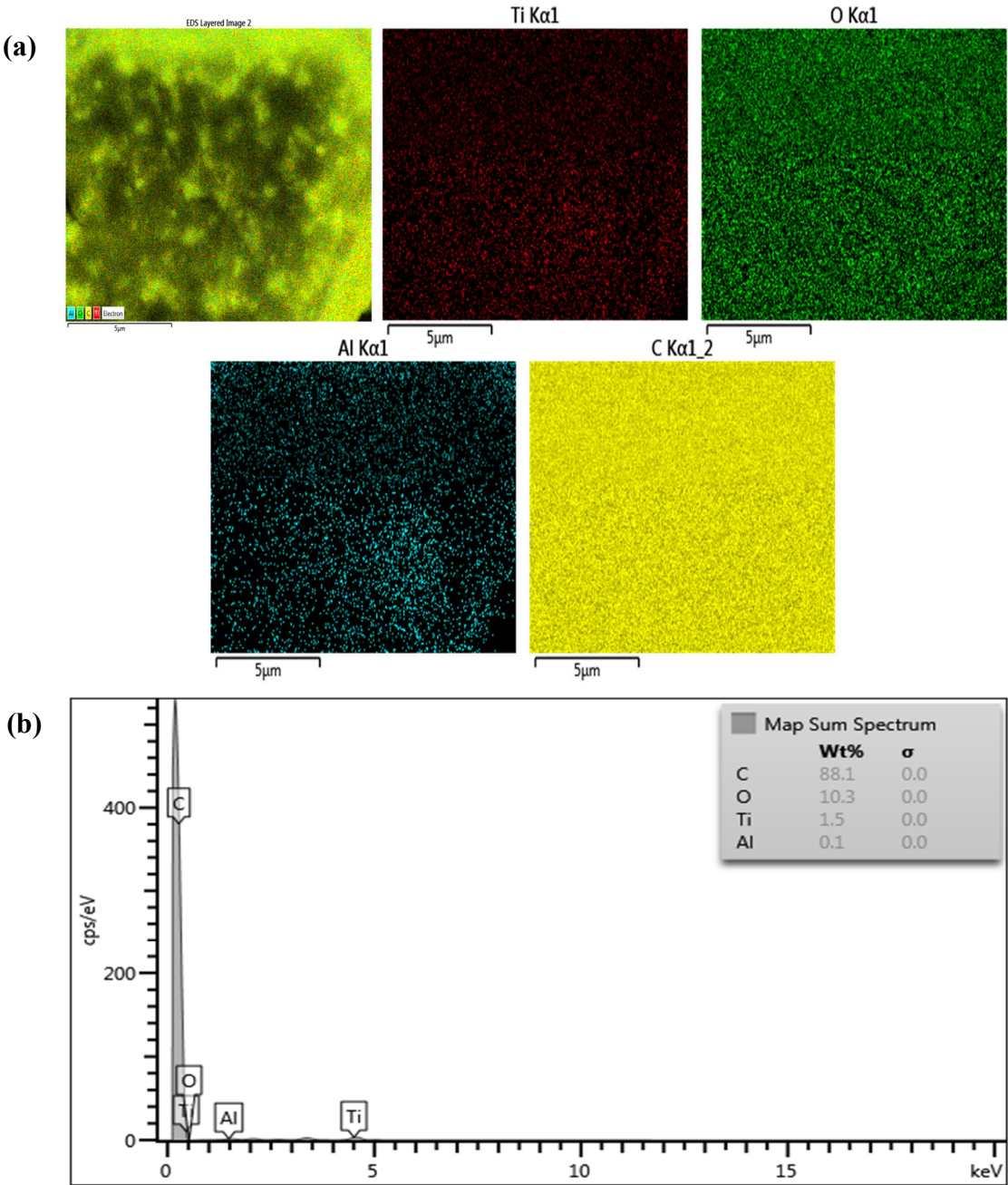


Figure 5. (a) Elemental mapping (elements: Ti, C, O, Al) of $\text{Ti}_3\text{C}_2\text{T}_x$ -rGO composite, and (b) EDX of $\text{Ti}_3\text{C}_2\text{T}_x$ -rGO composite.

The chemical composition of the as-prepared $\text{Ti}_3\text{C}_2\text{T}_x\text{-rGO}$ composite was investigated via XPS analysis (Figure 6). $\text{Ti}2p$, $\text{C}1s$ and $\text{O}1s$ signals are obtained at the binding energy of 458, 285 and 529 eV, respectively (Figure 6(a)). $\text{Ti}2p$ signal originated from $\text{Ti}_3\text{C}_2\text{T}_x$ MXene, while $\text{C}1s$ and $\text{O}1s$ are produced by both $\text{Ti}_3\text{C}_2\text{T}_x$ and rGO. The $\text{Ti}2p_{1/2}$ and $\text{Ti}2p_{3/2}$ characteristics are observed from Figure 6(b). The deconvolution of $\text{Ti}2p$ spectrum depicts seven different peaks, which appear at the binding energy of 454.7 ($\text{Ti-C } 2p_{3/2}$), 455.2 (Ti(II)), 456.5 ($\text{Ti-O } 2p_{3/2}$), 459.2 (TiO_2), 461.1 ($\text{Ti-C } 2p_{1/2}$), 461.9 (Ti(III)), 463.3 eV ($\text{Ti-O } 2p_{1/2}$) [33-36]. The $\text{C}1s$ spectrum presented in Figure 6(c) illustrates four deconvoluted XPS peaks, which indicate the C=C/C-C , C-O (epoxy and hydroxy), C=O and O-C=O interactions happened at specific binding energies of 281.4, 282.1, 284.6 and 286.2 eV, respectively. From the result, it can be clearly seen that the intensity of C-C/C=C signal is relatively higher than the C-O (hydroxy and epoxy), revealing a successful reduction of GO and it also proves that the rGO within the composite still consist of several oxygen-containing functional groups [37]. The $\text{O}1s$ spectrum (Figure 6(d)) is deconvoluted into four peaks that are clearly noticed at the binding energy of 529.7 eV (O-Ti), 530.6 eV (C-Ti-O_x), 531.4 eV (C-Ti-OH_x) and 532.7 eV ($\text{H}_2\text{O-Ti}$) [33]. XPS result affirms that the $\text{Ti}_3\text{C}_2\text{T}_x$ MXene is successfully obtained via the chemical synthesis route. The electrochemical reduction effectively reduced GO to rGO without disturbing the structure of $\text{Ti}_3\text{C}_2\text{T}_x$ MXene. The XPS signal is also in full alignment with the XRD, FTIR, Raman, FESEM, EDX and elemental mapping results presented earlier.

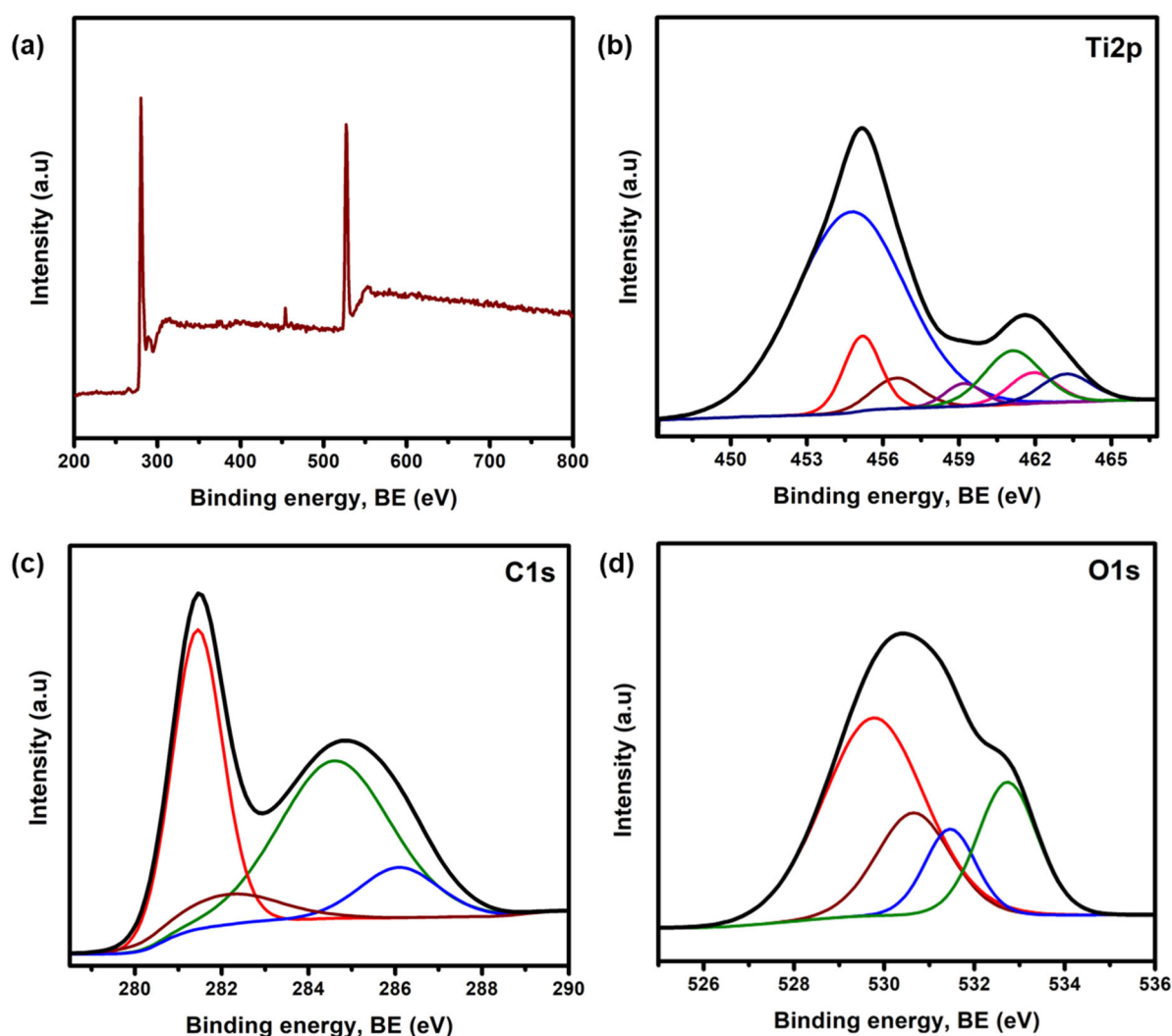


Figure 6. (a) Wide scan XPS spectra and the high resolution (b) $\text{Ti}2p$, (c) $\text{C}1s$, and (d) $\text{O}1s$, of $\text{Ti}_3\text{C}_2\text{T}_x\text{-rGO}$ composite.

3.2. Electrochemical Detection

Figure 7(a) depicts the DPV curve of bare GCE, rGO, $\text{Ti}_3\text{C}_2\text{T}_x$ MXene, and $\text{Ti}_3\text{C}_2\text{T}_x$ -rGO electrodes for the detection of 1 mM Cd^{2+} and Cu^{2+} in PBS solution (pH=5.0). An obvious and low intensity Cd^{2+} signal and a broad and weak Cu^{2+} peak is obtained for bare GCE at the respective values of -0.74 and -0.16 V. Comparatively, the Cd^{2+} ion peak current is noticeably higher than the Cu^{2+} ion, indicating the difference in sensitivity of electrode for both heavy metal ions. The introduction of $\text{Ti}_3\text{C}_2\text{T}_x$ or rGO on a bare GCE illustrates an evident spike in peak currents and increase in the electrochemical signal through instantaneous ions detection, caused by the higher electrocatalytic activity and electrochemical surface area. On the other hands, the pristine GCE, $\text{Ti}_3\text{C}_2\text{T}_x$ MXene demonstrates prominent absorption peaks at the respective -0.75 and -0.17 V that indicate the peak of Cd^{2+} and Cu^{2+} . Meanwhile, the Cu^{2+} signal is found weak for rGO. Therefore the integration of $\text{Ti}_3\text{C}_2\text{T}_x$ and rGO to form $\text{Ti}_3\text{C}_2\text{T}_x$ -rGO has resulted in greater peak currents as the rGO increased the interlayer spacing of $\text{Ti}_3\text{C}_2\text{T}_x$, created a greater surface area for the better interaction of Cd^{2+} and Cu^{2+} , with $\text{Ti}_3\text{C}_2\text{T}_x$ -rGO composite [38]. $\text{Ti}_3\text{C}_2\text{T}_x$ -rGO displays high intensity peak current than the $\text{Ti}_3\text{C}_2\text{T}_x$, rGO and bare GCE. Interestingly, $\text{Ti}_3\text{C}_2\text{T}_x$ -rGO shows completely separated and intense peak currents that improves the detection of Cu^{2+} and Cd^{2+} ions electrochemically. The synergistic effect within the $\text{Ti}_3\text{C}_2\text{T}_x$ -rGO electrode lead to outstanding oxidation signals towards Cd^{2+} and Cu^{2+} ions.

Figure 7(b) demonstrates the DPV of $\text{Ti}_3\text{C}_2\text{T}_x$ -rGO composite immersed in the PBS solution consisting of 1mM Cd^{2+} - Cu^{2+} within the pH range of 4.0 to 6.5. The peak potentials of Cd^{2+} - Cu^{2+} have shown slightly deviations to the negative potential as the pH of the PBS rises, which validated the redox reactions under the proton influence [39, 40]. This is because the presence of proton in the PBS solution reduces as the pH of the solvent rises. Cd^{2+} and Cu^{2+} ions rapidly form anion in the high pH PBS solution. The produced anion develops an electrostatic repulsion within Cd^{2+} , Cu^{2+} as well as $\text{Ti}_3\text{C}_2\text{T}_x$ -rGO, causing difficulty for electrochemical reaction to occur at high pH with low peak currents. Figure 7(c) illustrates the peak current versus pH of Cd^{2+} and Cu^{2+} . The peak currents for Cd^{2+} and Cu^{2+} intensified when the pH elevated from 4 to 5, potentially due to the competition between the targeted heavy metal ions and protons for the binding sites on the electrode surface [41]. This phenomenon is due to the increase of pH of the PBS, which have resulted in the amount of proton present in the analyte solution to decrease. This later caused the Cd^{2+} and Cu^{2+} ions to be easily oxidized and form anion easily at higher pH. The presence of these anions will cause an electrostatic repulsion between the heavy metal ions and the $\text{Ti}_3\text{C}_2\text{T}_x$ -rGO composite, resulting low peak current [40]. The Cd^{2+} and Cu^{2+} signals from pH 5.5 to 6.5 are observed with low peak currents, which is due to the hydrolysis of heavy metal ions [42, 43]. The ideal pH used for this task is pH 5 as it illustrates highest peak current of 51.4 and 3.47 μA for Cd^{2+} and Cu^{2+} , respectively. The relationship of the peak potential (E_p) of Cd^{2+} and Cu^{2+} versus pH is demonstrated in Figure 7(d-e). The E_p of both Cd^{2+} and Cu^{2+} are noticeably proportional to the PBS pH in accordance with the regression equation of E_p (V) = -0.046 pH - 0.637 ($R^2=0.989$) for Cd^{2+} and E_p (V) = -0.042 pH + 0.018 ($R^2=0.967$) for Cu^{2+} , respectively.

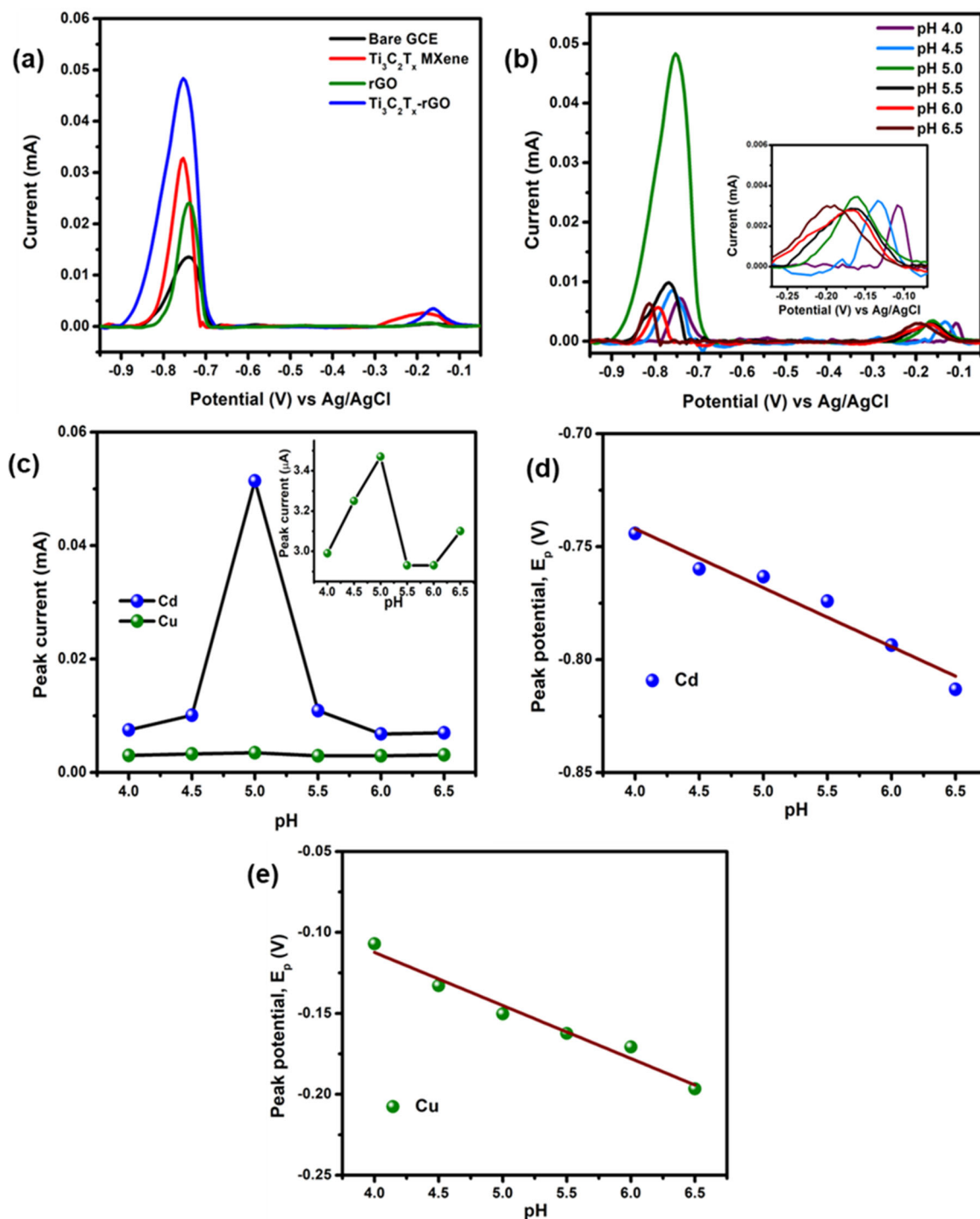


Figure 7. Differential pulse voltammogram of (a) various electroactive materials at pH 5 and (b) Ti₃C₂T_x-rGO composite in PBS solution (1mM Cd²⁺ and 1 mM Cu²⁺) altering the pH from 4 to 6.5. (c) PBS pH on the peak current of Cd²⁺ and Cu²⁺ effect (inset: detailed Cu peak current response against the pH) and impact of PBS pH on the peak potential of (d) Cd²⁺ and (e) Cu²⁺.

The simultaneous detection of Cd²⁺ and Cu²⁺ was performed via DPV analysis (Figure 8(a)) utilizing Ti₃C₂T_x-rGO. Figure 8(a) depicts the Cd²⁺ and Cu²⁺ ions detection in PBS solution (pH 5), varying the concentration of Cd²⁺ (7.5-150 nM) and Cu²⁺ (1-150 nM). Figure 8 (b) and (d) displays differential pulse voltammograms that focus on Ti₃C₂T_x-rGO composite in various Cd²⁺ and Cu²⁺ concentrations ranging from 7.5 to 150 nM and 1 to 150 nM, respectively. Result implies that the peak current of Cd²⁺ and Cu²⁺ increases with increasing concentration [44]. The plot of peak current against

concentration of Cd^{2+} and Cu^{2+} is exhibited in Figure 8 (c) and (e), respectively. The Cd^{2+} peak currents rise gradually with the concentration of Cd^{2+} and the correlation between peak current with Cd^{2+} concentration shall be potentially represented in the form of $I_{\text{pa}} (\mu\text{M})=0.345 \text{ Cd}^{2+} (\mu\text{M}) + 0.010$ with $R^2=0.999$. The sensitivity of $\text{Ti}_3\text{C}_2\text{T}_x\text{-rGO}$ against Cd^{2+} is $0.345 \mu\text{M}\mu\text{A}^{-1}$, which is attained from the slope of the equation. Similarly, the peak currents of Cu^{2+} constantly increases as the concentration of Cu^{2+} is rises. Cu^{2+} also shows a straight line curve of peak current and Cu^{2+} concentration, that is presented as $I_{\text{pa}} (\mu\text{M})=0.575 \text{ Cu}^{2+} (\mu\text{M}) + 0.158$ where $R^2=0.993$. The achieved sensitivity of $\text{Ti}_3\text{C}_2\text{T}_x\text{-rGO}$ towards the detection of Cu^{2+} is $0.575 \mu\text{M}\mu\text{A}^{-1}$. It can be concluded that the modified $\text{Ti}_3\text{C}_2\text{T}_x\text{-rGO}$ electrode is capable to demonstrate a complete-separation of oxidation peak and the electrochemical detection of Cd^{2+} and Cu^{2+} that does not interfere each other. Limit of detection (LOD) and limit of quantification (LOQ) is measured via Eq. (1) and (2), where σ and s are standard deviation and slope of the calibration curve, respectively. The LOD of $\text{Ti}_3\text{C}_2\text{T}_x\text{-rGO}$ modified electrode for Cd^{2+} and Cu^{2+} are 0.31 and 0.18 nM, respectively. Whereas, the LOQ discovered for Cd^{2+} and Cu^{2+} are 1.02 and 0.62 nM, respectively. The performance of the suggested composite and the other modified electrodes in detecting Cd^{2+} and Cu^{2+} is tabulated in Table 1. The $\text{Ti}_3\text{C}_2\text{T}_x\text{-rGO}$ composite result is comparable with the reported literature. The proposed electroactive material in this work also demonstrated an outstanding LOD for simultaneous heavy metals detection, which is significantly lower than the other reported MXene based composites.

$$LOD = \frac{3\sigma}{s}$$
 (Eq. 1)

$$LOQ = \frac{10\sigma}{s}$$
 (Eq. 2)

Table 1. Performance of various MXene-based electrodes for heavy metal detection.

No.	Material	Heavy metal detected	LOD (nM)	Linear range of detection (μM)	Reference
1	alk- Ti_3C_2	Cu^{2+}	39.00	0.1-1.4 μM	[45]
		Cd^{2+}	82.00	0.1-1.4 μM	
2	$\text{H-C}_3\text{N}_4/\text{Ti}_3\text{C}_2\text{T}_x$	Cd^{2+}	1.00	0.5-1.5 μM	[46]
		Pb^{2+}	0.60	0.5-1.5 μM	
3	$\text{Ti}_3\text{C}_2@\text{N-C}$	Cd^{2+}	2.25	0.1-4 μM	[47]
		Pb^{2+}	1.10	0.05-2 μM	
4	$\text{BiNPs}/\text{Ti}_3\text{C}_2\text{T}_x$	Cd^{2+}	12.4	0.08-0.8 μM	[48]
		Pb^{2+}	10.8	0.06-0.6 μM	
5	$\text{Ti}_3\text{C}_2\text{T}_x\text{-rGO}$	Cd^{2+}	0.31	7.5-150 nM	This work
		Cu^{2+}	0.18	1-150 nM	

alk- Ti_3C_2 : alkaline intercalation of Ti_3C_2 , $\text{H-C}_3\text{N}_4/\text{Ti}_3\text{C}_2\text{T}_x$: protonated carbon nitride/ $\text{Ti}_3\text{C}_2\text{T}_x$, $\text{Ti}_3\text{C}_2@\text{N-C}$: nitrogen-doped carbon-coated $\text{Ti}_3\text{C}_2\text{-MXene}$, $\text{BiNPs}/\text{Ti}_3\text{C}_2\text{T}_x$: bismuth-nanoparticles/ $\text{Ti}_3\text{C}_2\text{T}_x$.

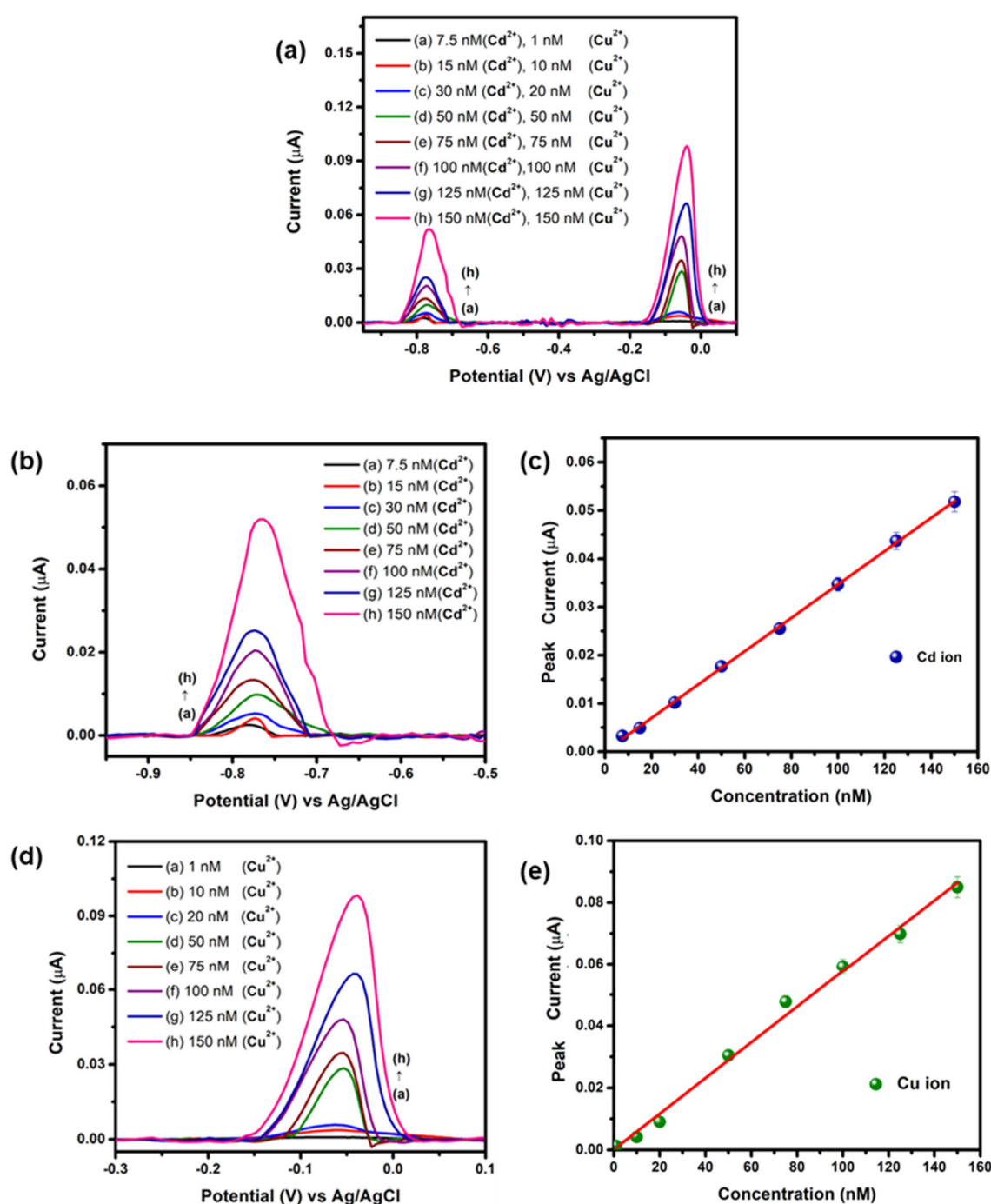


Figure 8. (a) DPV response of $\text{Ti}_3\text{C}_2\text{Tx-rGO}$ electrode for the detection of Cd^{2+} and Cu^{2+} in the PBS solution (pH 5). DPV plot of $\text{Ti}_3\text{C}_2\text{Tx-rGO}$ electrode at different concentrations for (b) Cd^{2+} (7.5-150 nM) and (d) Cu^{2+} (1-150 nM) detection with the calibration plot for both (c) Cd^{2+} and (e) Cu^{2+} with error bar: standard deviation for $n=3$.

The reproducibility of $\text{Ti}_3\text{C}_2\text{Tx-rGO}$ was determined by testing 0.5 mM Cd^{2+} and Cu^{2+} using five distinct electrodes and the calculated relative standard deviation (RSD) of 2.42% and 2.36% are attained for Cd^{2+} and Cu^{2+} , respectively. The repeatability of $\text{Ti}_3\text{C}_2\text{Tx-rGO}$, is evaluated for 10 DPV signal of an electrode and analysed in the 0.5 mM solution of Cd^{2+} and Cu^{2+} . The calculated RSD are 1.93% and 3.58% for Cd^{2+} and Cu^{2+} , respectively, signifying outstanding repeatability of the proposed material. The $\text{Ti}_3\text{C}_2\text{Tx-rGO}$ sensor constancy was determined upon testing 0.1 mM Cd^{2+} and 0.1 mM Cu^{2+} in the pH 5 PBS solution. Although the approximate concentration of dissolved oxygen in water

at room temperature and 1 atm pressure is around 0.25 mM, even nanomolar concentrations of metal ions can significantly suppress the oxygen signal observed in Differential Pulse Voltammetry (DPV). This seemingly disproportionate effect arises from several electrochemical and chemical interactions. Certain metal ions, such as Cu^{2+} , Fe^{2+} , or Mn^{2+} , can catalyze the oxygen reduction reaction (ORR), altering the kinetics and mechanisms of oxygen's electrochemical behaviors. These ions can form transient complexes with oxygen or its reduction intermediates, thereby modifying the redox potential and diminishing the distinct oxygen peak in DPV. Additionally, metal ions can adsorb onto the electrode surface and alter its electrochemical properties, including electron transfer rates and surface reactivity. This surface modification can hinder the reduction of oxygen or shift its peak, leading to apparent suppression. Despite their low concentration, these ions can exert a catalytic or surface-blocking effect that disrupts the sensitivity and resolution of DPV, which is a highly sensitive technique designed to detect subtle changes in current. Thus, the suppression of oxygen signals by trace metal ions highlights the importance of understanding both direct and indirect interactions in electrochemical analyses.

Next, the prepared sensor was stored for 30 days at atmospheric temperature and the detailed peak current retention (%) of $\text{Ti}_3\text{C}_2\text{T}_x\text{-rGO}$ is tabulated in Table 2. Result shows that $\text{Ti}_3\text{C}_2\text{T}_x\text{-rGO}$ electrode retained 97.86% (Cd^{2+}) and 98.01% (Cu^{2+}) of its initial peak current responses, implying excellent stability of $\text{Ti}_3\text{C}_2\text{T}_x\text{-rGO}$ towards simultaneous detection Cd^{2+} and Cu^{2+} .

Table 2. Stability study of $\text{Ti}_3\text{C}_2\text{T}_x\text{-rGO}$ electrode for the detection of Cd^{2+} and Cu^{2+} .

Stability period	Peak current retention (%)	
	Cd^{2+}	Cu^{2+}
1 Week	98.19%	99.81%
2 Week	98.61%	99.48%
3 Week	99.89%	98.49%
4 Week	97.86%	98.01%

The impact of various interference ions in the PBS containing 1 mM Cd^{2+} and Cu^{2+} were investigated using $\text{Ti}_3\text{C}_2\text{T}_x\text{-rGO}$. The 100- fold and 1000-fold concentration of the interference ions (Na^+ , K^+ , Ca^{2+} , Mg^{2+} , Cl^- , SO_4^{2-}) were tested and the result shows that the injected ions do not interfere the simultaneous detection of Cd^{2+} and Cu^{2+} ions in PBS (pH = 5) where the signal change is less than 5% [40]. The excellent interference resistance disclosed that $\text{Ti}_3\text{C}_2\text{T}_x\text{-rGO}$ is reliable even under ambient conditions. The practical effectiveness of $\text{Ti}_3\text{C}_2\text{T}_x\text{-rGO}$ for simultaneous Cd^{2+} and Cu^{2+} detection has been explored employing lake water and tap water. A predetermined quantity of Cd^{2+} and Cu^{2+} was injected into the solution for the purpose of the recovery experiment, which was carried out using DPV analysis. The quantity of Cd^{2+} and Cu^{2+} found in lake and supplied drinking water was identified using the traditional addition technique, and the recovery of Cd^{2+} and Cu^{2+} in percentage were ranged between 96% and 99.5% (Tables 3 and 4). The results show that the $\text{Ti}_3\text{C}_2\text{T}_x\text{-rGO}$ composite is capable of detecting Cd^{2+} and Cu^{2+} simultaneously using actual water samples.

Table 3. Recovery data on concurrent detection of Cd^{2+} and Cu^{2+} in lake water (n=3).

Sample	Added (nM)		Obtained (nM)		Recovery (%)	
	Cd^{2+}	Cu^{2+}	Cd^{2+}	Cu^{2+}	Cd^{2+}	Cu^{2+}
1	60	60	58.4	58.9	97.3%	98.2%
2	80	80	78.1	79.3	97.6%	99.1%
3	100	100	98.9	99.5	98.9%	99.5%

Table 4. Recovery data on concurrent detection of Cd^{2+} and Cu^{2+} in tap water (n=3).

Sample	Added (nM)	Obtained (nM)	Recovery (%)
--------	------------	---------------	--------------

	Cd ²⁺	Cu ²⁺	Cd ²⁺	Cu ²⁺	Cd ²⁺	Cu ²⁺
1	60	60	58.7	57.6	97.8%	96.0%
2	80	80	78.2	78.3	97.8%	97.9%
3	100	100	99	98.8	99.0%	98.8%

4. Conclusions

A promising Ti₃C₂T_x-rGO sensor for Cd²⁺ and Cu²⁺ detection was successfully developed employing chemically synthesized Ti₃C₂T_x and electrochemically produced rGO by demonstrating obvious and intense Cd²⁺ and Cu²⁺ oxidation peaks via DPV analysis. Ti₃C₂T_x-rGO composite revealed a significant electro-chemical-catalytic activity with respect to the Cd²⁺ and Cu²⁺ oxidation. It is also found that improved electron transfer characteristics in comparison to the bare GCE, Ti₃C₂T_x and rGO. Ti₃C₂T_x-rGO sensor were obtained. The results demonstrated a significantly low LOD and LOQ for concurrent detection of Cd²⁺ (LOD = 0.31 nM, LOQ = 1.02 nM) and Cu²⁺ (LOD = 0.18 nM, LOQ = 0.62 nM) ions in water. The promising Ti₃C₂T_x-rGO electrode illustrated excellent sensitivity of 0.345 and 0.575 $\mu\text{M}\mu\text{A}^{-1}$ for Cd²⁺ and Cu²⁺ ions, respectively. Ti₃C₂T_x-rGO composite also disclose promising duplicability, repeatability, and consistency of Cd²⁺ and Cu²⁺ detection. Thus, Ti₃C₂T_x-rGO is proven as an outstanding electrochemical sensor for identifying Cd²⁺ and Cu²⁺ successfully.

Acknowledgments: This work was supported and funded by the Deanship of Scientific Research at Imam Mohammad Ibn Saud Islamic University (IMSIU) (grant number IMSIU-DDRSP2502).

References

1. M.B. Gumpu, S. Sethuraman, U.M. Krishnan, J.B.B. Rayappan, A review on detection of heavy metal ions in water—an electrochemical approach, *Sensors and actuators B: chemical* 213 (2015) 515-533.
2. H. Yin, Q. Zhang, Y. Zhou, Q. Ma, L. Zhu, S. Ai, Electrochemical behavior of catechol, resorcinol and hydroquinone at graphene-chitosan composite film modified glassy carbon electrode and their simultaneous determination in water samples, *Electrochim. Acta* 56 (2011) 2748-2753.
3. A.J.S. Ahammad, M.M. Rahman, G.-R. Xu, S. Kim, J.-J. Lee, Highly sensitive and simultaneous determination of hydroquinone and catechol at poly (thionine) modified glassy carbon electrode, *Electrochimica Acta* 56 (2011) 5266-5271.
4. Y. Yi, Y. Zhao, Z. Zhang, Y. Wu, G. Zhu, Recent developments in electrochemical detection of cadmium, *Trends in Environmental Analytical Chemistry* 33 (2022) e00152.
5. A. Shahzad, K. Rasool, W. Miran, M. Nawaz, J. Jang, K.A. Mahmoud, D.S. Lee, Two-dimensional Ti₃C₂T_x MXene nanosheets for efficient copper removal from water, *ACS Sustainable Chemistry & Engineering* 5 (2017) 11481-11488.
6. Y. Yi, Y. Ma, F. Ai, Y. Xia, H. Lin, G. Zhu, Novel methodology for anodic stripping voltammetric sensing of heavy-metal ions using Ti₃C₂T_x nanoribbons, *Chemical Communications* 57 (2021) 7790-7793.
7. Q. Peng, J. Guo, Q. Zhang, J. Xiang, B. Liu, A. Zhou, R. Liu, Y. Tian, Unique lead adsorption behavior of activated hydroxyl group in two-dimensional titanium carbide, *J. Am. Chem. Soc.* 136 (2014) 4113-4116.
8. Y. Xia, Y. Ma, Y. Wu, Y. Yi, H. Lin, G. Zhu, Free-electrodeposited anodic stripping voltammetry sensing of Cu (II) based on Ti₃C₂T_x MXene/carbon black, *Microchimica Acta* 188 (2021) 1-9.
9. Y. Xia, Y. Zhao, F. Ai, Y. Yi, T. Liu, H. Lin, G. Zhu, N and P co-doped MXenes nanoribbons for electrodeposition-free stripping analysis of Cu (II) and Hg (II), *Journal of Hazardous Materials* 425 (2022) 127974.
10. A. Maity, X. Sui, C.R. Tarman, H. Pu, J. Chang, G. Zhou, R. Ren, S. Mao, J. Chen, Pulse-driven capacitive lead ion detection with reduced graphene oxide field-effect transistor integrated with an analyzing device for rapid water quality monitoring, *ACS sensors* 2 (2017) 1653-1661.
11. K. Hamsawahini, P. Sathishkumar, R. Ahamad, A.R.M. Yusoff, A sensitive, selective and rapid determination of lead (II) ions in real-life samples using an electrochemically reduced graphene oxide-graphite reinforced carbon electrode, *Talanta* 144 (2015) 969-976.

12. X. Xuan, M. Hossain, J.Y. Park, A fully integrated and miniaturized heavy-metal-detection sensor based on micro-patterned reduced graphene oxide, *Scientific reports* 6 (2016) 1-8.
13. S. Wu, K. Zhang, X. Wang, Y. Jia, B. Sun, T. Luo, F. Meng, Z. Jin, D. Lin, W. Shen, Enhanced adsorption of cadmium ions by 3D sulfonated reduced graphene oxide, *Chem. Eng. J.* 262 (2015) 1292-1302.
14. D. Mohanadas, N.H.N. Azman, J. Abdullah, N.A. Endot, Y. Sulaiman, Bifunctional ternary manganese oxide/vanadium oxide/reduced graphene oxide as electrochromic asymmetric supercapacitor, *Ceram. Int.* 47 (2021) 34529-34537.
15. D. Mohanadas, N.H.N. Azman, Y. Sulaiman, A bifunctional asymmetric electrochromic supercapacitor with multicolor property based on nickel oxide/vanadium oxide/reduced graphene oxide, *Journal of Energy Storage* 48 (2022) 103954.
16. A. Sengupta, B.B. Rao, N. Sharma, S. Parmar, V. Chavan, S.K. Singh, S. Kale, S. Ogale, Comparative evaluation of MAX, MXene, NanoMAX, and NanoMAX-derived-MXene for microwave absorption and Li ion battery anode applications, *Nanoscale* 12 (2020) 8466-8476.
17. X. Li, Y. Qian, T. Liu, F. Cao, Z. Zang, X. Sun, S. Sun, Q. Niu, J. Wu, Enhanced lithium and electron diffusion of LiFePO₄ cathode with two-dimensional Ti₃C₂ MXene nanosheets, *Journal of Materials Science* 53 (2018) 11078-11090.
18. H. Fang, Y. Pan, M. Yin, C. Pan, Enhanced visible light photocatalytic activity of CdS with alkalized Ti₃C₂ nano-sheets as co-catalyst for degradation of rhodamine B, *Journal of Materials Science: Materials in Electronics* 30 (2019) 14954-14966.
19. D. Mohanadas, M.A.A.M. Abdah, N.H.N. Azman, T.B. Ravooof, Y. Sulaiman, Facile synthesis of PEDOT-rGO/HKUST-1 for high performance symmetrical supercapacitor device, *Scientific reports* 11 (2021) 1-13.
20. S. Bai, X. Shen, X. Zhong, Y. Liu, G. Zhu, X. Xu, K. Chen, One-pot solvothermal preparation of magnetic reduced graphene oxide-ferrite hybrids for organic dye removal, *Carbon* 50 (2012) 2337-2346.
21. S.-X. Wang, H. Maimaiti, B. Xu, A. Awati, G.-B. Zhou, Y.-d. Cui, Synthesis and visible-light photocatalytic N₂/H₂O to ammonia of ZnS nanoparticles supported by petroleum pitch-based graphene oxide, *Appl. Surf. Sci.* 493 (2019) 514-524.
22. Z. Gohari-Bajestani, O. Akhlaghi, Y. Yürüm, A. Yürüm, Synthesis of anatase TiO₂ with exposed (001) facets grown on N-doped reduced graphene oxide for enhanced hydrogen storage, *Int. J. Hydrogen Energy* 42 (2017) 6096-6103.
23. M. Huang, J. Yu, Q. Hu, W. Su, M. Fan, B. Li, L. Dong, Preparation and enhanced photocatalytic activity of carbon nitride/titania (001 vs 101 facets)/reduced graphene oxide (g-C₃N₄/TiO₂/rGO) hybrids under visible light, *Appl. Surf. Sci.* 389 (2016) 1084-1093.
24. J. Xu, Q. Liang, Z. Li, V.Y. Osipov, Y. Lin, B. Ge, Q. Xu, J. Zhu, H. Bi, Rational Synthesis of Solid-State Ultraviolet B Emitting Carbon Dots via Acetic Acid-Promoted Fractions of sp³ Bonding Strategy, *Adv. Mater.* 34 (2022) 2200011.
25. Y. Chen, S. Yang, J. Zhang, The chemical composition and bonding structure of B-C-N-H thin films deposited by reactive magnetron sputtering, *Surface and Interface Analysis: An International Journal devoted to the development and application of techniques for the analysis of surfaces, interfaces and thin films* 41 (2009) 865-871.
26. D. Mohanadas, M.A.A.M. Abdah, N.H.N. Azman, J. Abdullah, Y. Sulaiman, A promising negative electrode of asymmetric supercapacitor fabricated by incorporating copper-based metal-organic framework and reduced graphene oxide, *Int. J. Hydrogen Energy* 46 (2021) 35385-35396.
27. S.L. Rebelo, A. Guedes, M.E. Szeftczyk, A.M. Pereira, J.P. Araújo, C. Freire, Progress in the raman spectra analysis of covalently functionalized multiwalled carbon nanotubes: unraveling disorder in graphitic materials, *PCCP* 18 (2016) 12784-12796.
28. L. Lorencova, T. Bertok, E. Dosekova, A. Holazova, D. Paprckova, A. Vikartovska, V. Sasinkova, J. Filip, P. Kasak, M. Jerigova, Electrochemical performance of Ti₃C₂T_x MXene in aqueous media: towards ultrasensitive H₂O₂ sensing, *Electrochim. Acta* 235 (2017) 471-479.
29. Y.-Y. Yang, W.-T. Zhou, W.-L. Song, Q.-Q. Zhu, H.-J. Xiong, Y. Zhang, S. Cheng, P.-F. Luo, Y.-W. Lu, Terminal Groups-Dependent Near-Field Enhancement Effect of Ti₃C₂T_x Nanosheets, *Nanoscale Research Letters* 16 (2021) 1-7.

30. S. Khasim, A. Pasha, N. Badi, M. Lakshmi, Y.K. Mishra, High performance flexible supercapacitors based on secondary doped PEDOT–PSS–graphene nanocomposite films for large area solid state devices, *RSC Advances* 10 (2020) 10526-10539.
31. B. Genorio, K.L. Harrison, J.G. Connell, G. Dražić, K.R. Zavadil, N.M. Markovic, D. Strmcnik, Tuning the selectivity and activity of electrochemical interfaces with defective graphene oxide and reduced graphene oxide, *ACS applied materials & interfaces* 11 (2019) 34517-34525.
32. M. Gusain, R. Nagpal, MXene for solar cells, *Solar Energy Harvesting, Conversion, and Storage*, Elsevier 2023, pp. 171-200.
33. Y. Zhou, Y. Wang, Y. Wang, X. Li, Humidity-enabled ionic conductive trace carbon dioxide sensing of nitrogen-doped $\text{Ti}_3\text{C}_2\text{T}_x$ MXene/polyethyleneimine composite films decorated with reduced graphene oxide nanosheets, *Anal. Chem.* 92 (2020) 16033-16042.
34. A. Pazniak, P. Bazhin, N. Shplis, E. Kolesnikov, I. Shchetinin, A. Komissarov, J. Polcak, A. Stolin, D. Kuznetsov, $\text{Ti}_3\text{C}_2\text{T}_x$ MXene characterization produced from SHS-ground Ti_3AlC_2 , *Materials & Design* 183 (2019) 108143.
35. Q.T.H. Ta, N.M. Tran, J.-S. Noh, Rice crust-like $\text{ZnO}/\text{Ti}_3\text{C}_2\text{T}_x$ MXene hybrid structures for improved photocatalytic activity, *Catalysts* 10 (2020) 1140.
36. L. Yao, X. Tian, X. Cui, R. Zhao, X. Xiao, Y. Wang, Partially oxidized $\text{Ti}_3\text{C}_2\text{T}_x$ MXene-sensitive material-based ammonia gas sensor with high-sensing performances for room temperature application, *Journal of Materials Science: Materials in Electronics* 32 (2021) 27837-27848.
37. X. Ding, Y. Huang, S. Li, N. Zhang, J. Wang, FeNi_3 nanoalloy decorated on 3D architecture composite of reduced graphene oxide/molybdenum disulfide giving excellent electromagnetic wave absorption properties, *J. Alloys Compd.* 689 (2016) 208-217.
38. L. Jin, L. Chai, W. Yang, H. Wang, L. Zhang, Two-dimensional titanium carbides ($\text{Ti}_3\text{C}_2\text{T}_x$) functionalized by poly (m-phenylenediamine) for efficient adsorption and reduction of hexavalent chromium, *International Journal of Environmental Research and Public Health* 17 (2020) 167.
39. W. Ma, X. Yao, D. Sun, Simultaneous electrochemical determination of dopamine, epinephrine and uric acid at silver doped poly-L-cysteine film electrode, *Asian J. Chem* 25 (2013) 6625-6634.
40. D. Mohanadas, N. Tukimin, Y. Sulaiman, Simultaneous electrochemical detection of hydroquinone and catechol using poly (3, 4-ethylenedioxythiophene)/reduced graphene oxide/manganese dioxide, *Synth. Met.* 252 (2019) 76-81.
41. Y. El Hamdouni, S. El Hajjaji, T. Szabo, L. Trif, I. Felhősi, K. Abbi, N. Labjar, L. Harmouche, A. Shaban, Biomass valorization of walnut shell into biochar as a resource for electrochemical simultaneous detection of heavy metal ions in water and soil samples: Preparation, characterization, and applications, *Arabian Journal of Chemistry* 15 (2022) 104252.
42. H. Huang, T. Chen, X. Liu, H. Ma, Ultrasensitive and simultaneous detection of heavy metal ions based on three-dimensional graphene-carbon nanotubes hybrid electrode materials, *Anal. Chim. Acta* 852 (2014) 45-54.
43. Y.-Z. Tang, K.Y. Gin, M. Aziz, The relationship between pH and heavy metal ion sorption by algal biomass, *Adsorption Science & Technology* 21 (2003) 525-537.
44. N. Qu, D. Zhu, K.C. Chan, W. Lei, Pulse electrodeposition of nanocrystalline nickel using ultra narrow pulse width and high peak current density, *Surf. Coat. Technol.* 168 (2003) 123-128.
45. X. Zhu, B. Liu, H. Hou, Z. Huang, K.M. Zeinu, L. Huang, X. Yuan, D. Guo, J. Hu, J. Yang, Alkaline intercalation of Ti_3C_2 MXene for simultaneous electrochemical detection of Cd (II), Pb (II), Cu (II) and Hg (II), *Electrochim. Acta* 248 (2017) 46-57.
46. X. Lv, F. Pei, S. Feng, Y. Wu, S.-M. Chen, Q. Hao, W. Lei, Facile synthesis of protonated carbon nitride/ $\text{Ti}_3\text{C}_2\text{T}_x$ nanocomposite for simultaneous detection of Pb^{2+} and Cd^{2+} , *J. Electrochem. Soc.* 167 (2020) 067509.
47. X. Zhang, D. An, Z. Bi, W. Shan, B. Zhu, L. Zhou, L. Yu, H. Zhang, S. Xia, M. Qiu, Ti_3C_2 -MXene@ N-doped carbon heterostructure-based electrochemical sensor for simultaneous detection of heavy metals, *J. Electroanal. Chem.* 911 (2022) 116239.

48. Y. He, L. Ma, L. Zhou, G. Liu, Y. Jiang, J. Gao, Preparation and application of bismuth/MXene nano-composite as electrochemical sensor for heavy metal ions detection, *Nanomaterials* 10 (2020) 866.

Disclaimer/Publisher's Note: The statements, opinions and data contained in all publications are solely those of the individual author(s) and contributor(s) and not of MDPI and/or the editor(s). MDPI and/or the editor(s) disclaim responsibility for any injury to people or property resulting from any ideas, methods, instructions or products referred to in the content.